

08 Aug 2023

Behavior of Ultrahigh-Performance Concrete Plates Encasing Steel H-Piles

Mohamed ElGawady

Missouri University of Science and Technology, elgawadym@mst.edu

Binod Shrestha

Missouri University of Science and Technology, bsyb7@mst.edu

Follow this and additional works at: https://scholarsmine.mst.edu/civarc_enveng_facwork



Part of the [Architectural Engineering Commons](#), and the [Civil and Environmental Engineering Commons](#)

Recommended Citation

M. ElGawady and B. Shrestha, "Behavior of Ultrahigh-Performance Concrete Plates Encasing Steel H-Piles," *Transportation Research Record*, Aug 2023.

The definitive version is available at <https://doi.org/10.1177/03611981231185777>

This Article - Journal is brought to you for free and open access by Scholars' Mine. It has been accepted for inclusion in Civil, Architectural and Environmental Engineering Faculty Research & Creative Works by an authorized administrator of Scholars' Mine. This work is protected by U. S. Copyright Law. Unauthorized use including reproduction for redistribution requires the permission of the copyright holder. For more information, please contact scholarsmine@mst.edu.

Behavior of Ultrahigh-Performance Concrete Plates Encasing Steel H-Piles

Binod Shrestha¹ , Ahmed Gheni² , Mohanad M. Abdulazeez¹ ,
and Mohamed A. ElGawady¹ 

Transportation Research Record
1–16

© National Academy of Sciences:
Transportation Research Board 2023
Article reuse guidelines:

sagepub.com/journals-permissions
DOI: 10.1177/03611981231185777

journals.sagepub.com/home/trr



Abstract

Steel H-piles are exposed during their service life to wet-dry cycles in combination with salts, such as deicing, that may result in corrosion, leading to cross-sectional loss and reduction in axial load-carrying capacity. This paper proposes an innovative repair method for corroded steel H-piles using ultrahigh-performance concrete (UHPC) plates. The UHPC plates are reinforced with carbon fiber-reinforced polymer (CFRP) grids. The UHPC plates bridge the corroded segment so that the axial force bypasses the corroded segment. The UHPC are bolted to the steel H-pile using high-strength bolt connectors (HSBCs). Eleven steel H-piles bolted with UHPC plates were investigated experimentally under push-out loading to quantify the axial force that can be transferred from a steel H-pile to UHPC plates through HSBCs. The examined parameters were the UHPC plate thickness, the diameter of HSBC, and the number of CFRP grid layers. The results were compared with those predicted using different design codes and guidelines. The UHPC plates attached to the steel H-pile could transfer axial loads ranging from 35% to 98% of the steel H-piles' ultimate axial capacity. Further, the installation of the UHPC plate on a steel pile can be completed in about 2 h with minimal equipment, making it a promising repair candidate in real-world applications.

Keywords

infrastructure, construction, bridges and structures, ultrahigh performance concrete, metal structure fabrication and inspection, steel bridges, corrosion-damaged

Steel H-piles, particularly near wet areas, are exposed to periodic wet-dry cycles and salts from the surrounding environment (e.g., deicing or soil), resulting in localized corrosion near the soil or water surfaces. This corrosion triggers section loss, which reduces the axial and bending capacity of the corroded steel H-pile, impairing the overall strength of the supporting structure (1–3). To address this challenge, repairing methods have been proposed, including attaching welded or bolted steel plates and cast-in-place concrete encasement with or without fiber-reinforced polymer (FRP) jackets (4–7). However, the addition of steel plates is inherently susceptible to corrosion, and the concrete encasement is challenging for field implementation, especially underwater, as it requires on-site casting and curing along with reinforcement, temporary support, and formwork.

Recently, ultrahigh-performance concrete (UHPC) has been proposed to address the challenges associated with repairing and constructing infrastructure. UHPC

has a densely packed microstructure which makes it well-suited for applications in harsh environments. UHPC also has ultrahigh strength (8–12), low permeability and reduced porosity, high durability (13), resistance to corrosion and carbonation, low shrinkage and creep (14), and high toughness and impact resistance (15).

While several research projects have focused on mixture design and mechanical properties of UHPC (8, 11, 16–19), quite a few studies address the structural performance of UHPC components and elements. Hollow UHPC segments were used in the plastic hinges of bridge columns to improve their seismic performance and

¹Department of Civil, Architectural and Environmental Engineering, Missouri University of Science and Technology, Rolla, MO

²Department of Civil Engineering, Komar University of Science and Technology, Sulaymaniyah, Iraq

Corresponding Author:

Mohamed A. ElGawady, elgawady@mst.edu

accelerate bridge construction (20). UHPC was also used to repair bridge columns under the combined effect of constant axial and cyclic lateral loads (21, 22). Several studies investigated the structural behavior of prestressed UHPC beams (23–26) and the feasibility study of applying UHPC in bridge decks (27). The shear behavior of UHPC girders was also investigated (28–33). Increasing the volume fraction of steel fibers improves the torsional cracking and ultimate strengths of UHPC beams (34). The performance of corroded steel girders, repaired using UHPC subjected to gravity loads, was also examined (35, 36). The research on the application of UHPC in structural elements such as columns, beams, beam-to-column joints, and girders displayed an excellent structural response, whether in new construction or repair.

Precast UHPC plates were proposed to repair corroded steel H-piles (37). The plates were used to bridge the corroded H-pile sections. Precast plates are produced under controlled conditions, ensuring high-quality assurance. The used UHPC plates are easy and fast to install as this eliminates the on-site casting and curing and the need for formwork; the plates can be installed on one pile in about 2 h. Installation time is crucial when considering associated road closure times, traffic congestion, delays, and detours during the on-site repair work (38, 39). The plates were reinforced using carbon fiber-reinforced polymer (CFRP) grids to avoid potential corrosion.

There is limited research into the shear transfer between steel elements, precast UHPC plates, and steel and precast high-strength steel fiber concrete plates (37, 40–45). This research has revealed that the shear transfer between the precast plates and steel elements could be improved by increasing the tensile strength and the diameter of the bolt connectors, the thickness of the concrete plate, and the compressive strength of the used concrete. It was recommended that plate thickness in the range of 2–4 in. (50–100 mm) be used. Fang et al. (42) conducted 18 push-out tests on H-shaped steel beams encased in precast UHPC plates. It was recommended that 3-in. (75-mm) thick precast UHPC plates be used in combination with Grade 8.8 bolts having a diameter greater than 0.87 in. (22 mm). The proposed UHPC thickness was 1 in. (25 mm) smaller than that required for normal-strength conventional and geopolymer concrete plates (44, 46). In those studies (42, 44, 46), the precast plates were attached to the outer side of each flange, which created a local eccentricity at the steel flange-concrete plate resulting in combined shear-moment demand on the bolts instead of pure shear.

Research Significance

This study presents a method for the repair of corroded steel H-pile using precast UHPC plates. The UHPC plates sandwich the flanges along the piles' corroded

segments and extend to uncorroded sections, where they are installed using high-strength bolt connectors (HSBCs), that is, the axial load bypasses the corroded segment transferring through the UHPC plates. While the proposed method is promising, no experimental verification or specific design guidance exists for cast-in-place or post-installed anchors in UHPC concrete. Design standards such as AASHTO LRFD- bridge design specification (47) and ACI 318 (48) provide shear strength design equations for steel anchors in normal-strength concrete, that is, having compressive strength (f'_c) less than 10 ksi (69 MPa). However, no such equations were developed for steel anchors in UHPC. This paper presents push-out tests on 11 full-scale steel H-piles to quantify the axial force that can be transferred from a steel H-pile to UHPC plates through HSBCs.

Experimental Program

Test Specimens

Eleven HP10 × 42 steel H-piles with precast UHPC plates attached to their flanges using HSBC (Table 1) were subjected to push-out loading (Figure 1). The test parameters included the UHPC plate thickness (t_{UHPC}), the diameter of the HSBC, and the number of CFRP grid layers in each UHPC plate. Each UHPC plate was 12 × 17 in. (304.8 × 432 mm) with a thickness ranging from 0.75 to 2.25 in. (19 to 57 mm). The dimensions of the UHPC plates were kept minimal such that the weight of the plates remained appropriate for handling by two workers on a construction site while satisfying the structural function of the plates. Minimizing the size of the plates will also reduce the required construction material and repair cost.

Each UHPC plate was reinforced with one, two, or four layers of the CFRP grids (Figure 1*b-d*). In the case of four layers of the CFRP grids, each two CFRP layers were bundled together (Figure 1*d*). Four HSBCs, arranged in two rows, having a 0.5-in. (12.7-mm), 0.75-in. (19-mm), or 1-in. (25.4-mm) diameter, were used to attach each UHPC plate to the flange of each steel H-pile.

The test specimens (Table 1) were labeled as follows: (#)t, indicating the UHPC plate thickness in inches, (#)D, referring to the diameter of the HSBC in inches, which is followed by (#)G, the number of CFRP grid layers. For example, 0.75t-1/2D-2G was 0.75-in. (19-mm) thick UHPC plates, each reinforced using two CFRP grid layers and attached to a steel pile using 0.5-in. (12.7-mm) diameter HSBC.

Material Properties

Steel H-Pile. Three dog-bone coupons were cut from each web and one flange of a steel H-pile. The coupons were

Table 1. Test Parameters

Specimen designation	UHPC thickness (t_{UHPC}) (in. [mm])	HSBC diameter (d_b) (in. [mm])	No. of CFRP layers	Test set-up
A				
0.75t-1/2D-1G	0.75 (19)	0.5 (12.7)	1	UTM
1.5t-1/2D-1G	1.5 (38)		1	UTM
2.25t-1/2D-1G	2.25 (57)		1	UTM
2.25t-1/2D-2G	2.25 (57)		2	UTM
B				
2.25t-3/4D-1G*	2.25 (57)	0.75 (19)	1	SSTF
2.25t-3/4D-2G*	2.25 (57)		2	SSTF
2.25t-3/4D-4G*	2.25 (57)		4	SSTF
C				
0.75t-1D-1G	0.75 (19)	1 (25.4)	1	UTM
1.5t-1D-1G	1.5 (38)		1	UTM
2.25t-1D-1G*	2.25 (57)		1	SSTF
2.25t-1D-2G*	2.25 (57)		2	SSTF

Note: UHPC = ultrahigh-performance concrete; HSBC = high-strength bolt connectors; CFRP = carbon fiber-reinforced polymer; UTM = universal testing machine; SSTF = self-sustained testing frame.

*A specimen has an anticipated strength higher than the UTM capacity.

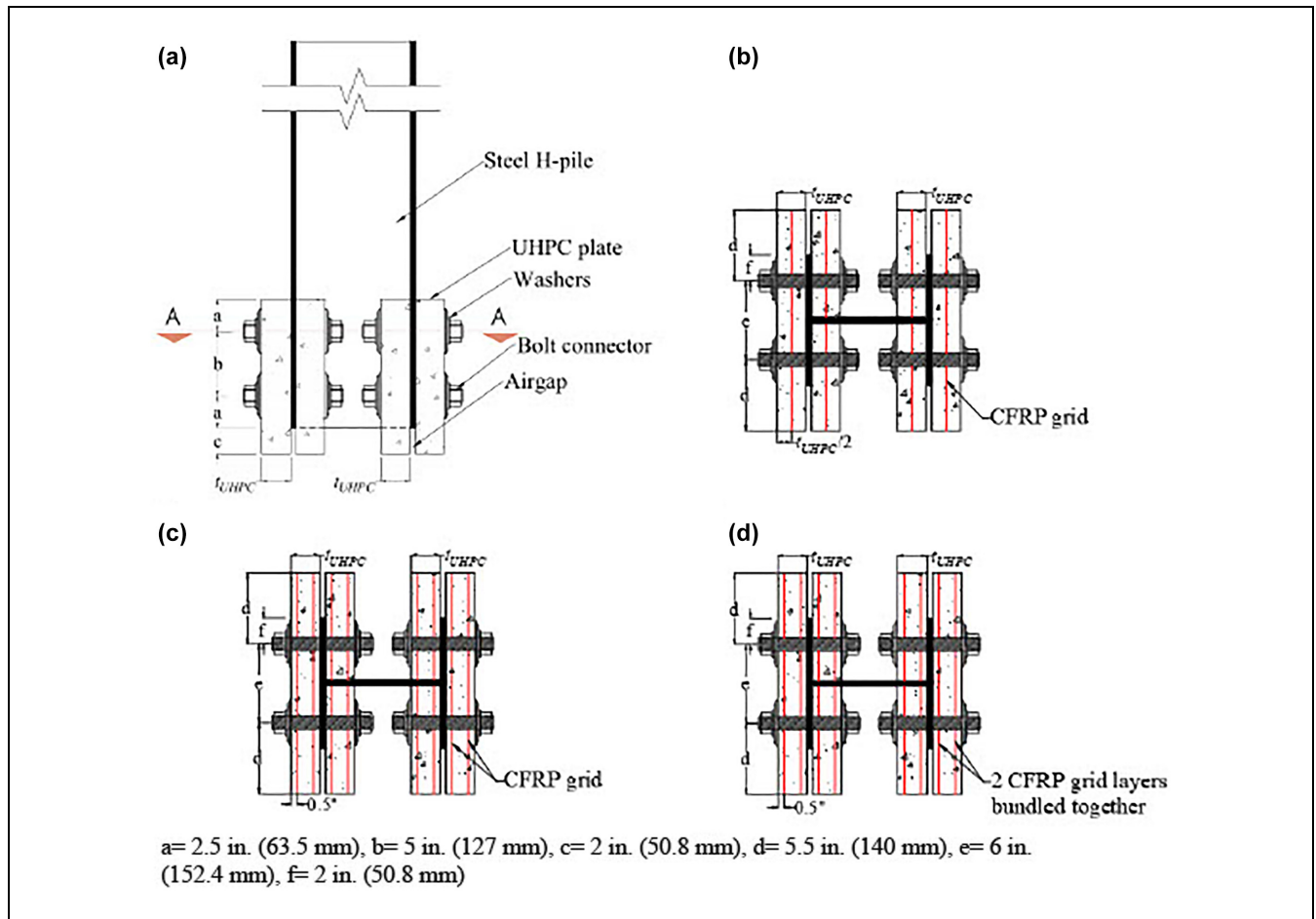


Figure 1. A UHPC repaired test specimen: (a) layout and section A-A indicating specimens reinforced with (b) one, (c) two, and (d) four layers of CFRP grids, respectively.

Note: UHPC = ultrahigh-performance concrete; CFRP = carbon fiber-reinforced polymer.

Table 2. Mechanical Properties of the Steel H-Pile

Section	Yield stress (ksi [MPa])	Ultimate stress (ksi [MPa])	Elastic modulus (ksi [GPa])	Rupture strain (in./in. [mm/mm])
Web	59 (407)	73 (503)	26,400 (182)	0.087
Flange	47 (324)	75 (517)	26,250 (181)	0.098

Note: ksi = kips per square inch.

Table 3. Mix Design of the UHPC

Cement Type III (lb/yd ³ [kg/m ³])	Slag (lb/yd ³ [kg/m ³])	Fine Sand (lb/yd ³ [kg/m ³])	HRWR (lb/yd ³ [kg/m ³])	Steel Fiber (lb/yd ³ [kg/m ³])	Water (lb/yd ³ [kg/m ³])	w/c*
1,593 (945)	371 (220)	1,699 (1,008)	74 (44)	265 (157)	337 (200)	0.2

Note: UHPC = ultrahigh-performance concrete; HRWR = high-range water reducer; w/c = water content.

*Ratio of total liquid (water content in HRWR and water) to the cementitious materials (cement and slag).

Table 4. Mechanical Properties of CFRP Grids per the Manufacturer's Data

Direction	Tensile strength per unit width (lb/ft [kN/m])	Elastic modulus (ksi [GPa])	Elongation at break (%)
Transverse	5,480 (79.9)	34,000 (234.5)	0.76
Longitudinal	5,530 (80.75)	34,000 (234.5)	0.76

Note: ksi = kips per square inch; CFRP = carbon fiber-reinforced polymer.

tested according to ASTM E8/E8M-16a (49). The average of three replicate coupons was taken to determine the tensile strength and E-modulus (Table 2).

Ultrahigh-Performance Concrete (UHPC). The UHPC mix consisted of high early strength cement type III, ground granulated blast furnace slag, fine masonry sand, polycarboxylate high-range water reducer (HRWR), straight micro steel fibers, and water (Table 3). A straight micro-fiber having a volume fraction of 2% of the total UHPC volume, a diameter of 0.0079 in. (0.2 mm), a length of 0.51 in. (13 mm), an elastic modulus of 29,443 ksi (203 GPa), and tensile strength of 275.57 ksi (1.9 GPa) was used to improve the ductility of the UHPC concrete and minimize its tensile cracks. The HRWR, having 23% solid mass content, was used to improve the workability of the UHPC.

The UHPC mixing was carried out using an Eirich mixer at an ambient temperature of $73 \pm 3^\circ\text{F}$ ($23 \pm 2^\circ\text{C}$). The fine sand and steel fibers were blended into the mixer for about two min, followed by gradual addition and mixing of about 50% of the total water for another two min. Then, cement and slags were added and mixed for 3 min. The remaining water, mixed with HRWR, was added. The mixing was then carried out for an additional 8 min until a homogenous UHPC mix was

developed. A mini-slump flow spread test per ASTM C1437 was carried out to measure the concrete flowability, which ranged from 10 in. (254 mm) to 12 in. (304 mm) (50).

High-Strength Bolt Connectors (HSBCs). Grade ASTM A490 (57) HSBCs with a minimum tensile strength of 150 ksi (1,034.2 MPa) were used. The HSBCs had three different diameters of 0.5 in. (12.7 mm), 0.75 in. (19.1 mm), and 1 in. (25.4 mm) and were installed on the steel H-piles using heavy-hex nuts.

Carbon Fiber-Reinforced Polymer (CFRP) Grids. The nominal spacings of each CFRP grid in the transverse and longitudinal directions were 1.6 in. (41 mm) and 1.8 in. (46 mm), respectively. Table 4 shows the mechanical properties per unit width of the CFRP grids as provided by the manufacturer.

Preparation of Test Specimens

The surface of a steel H-pile was cleaned using power hand tools to remove dust, dirt, and rust in accordance with the Society for Protective Coatings Standards (52). The required holes were drilled on the flanges of the steel H-piles to attach the UHPC plates using HSBCs.

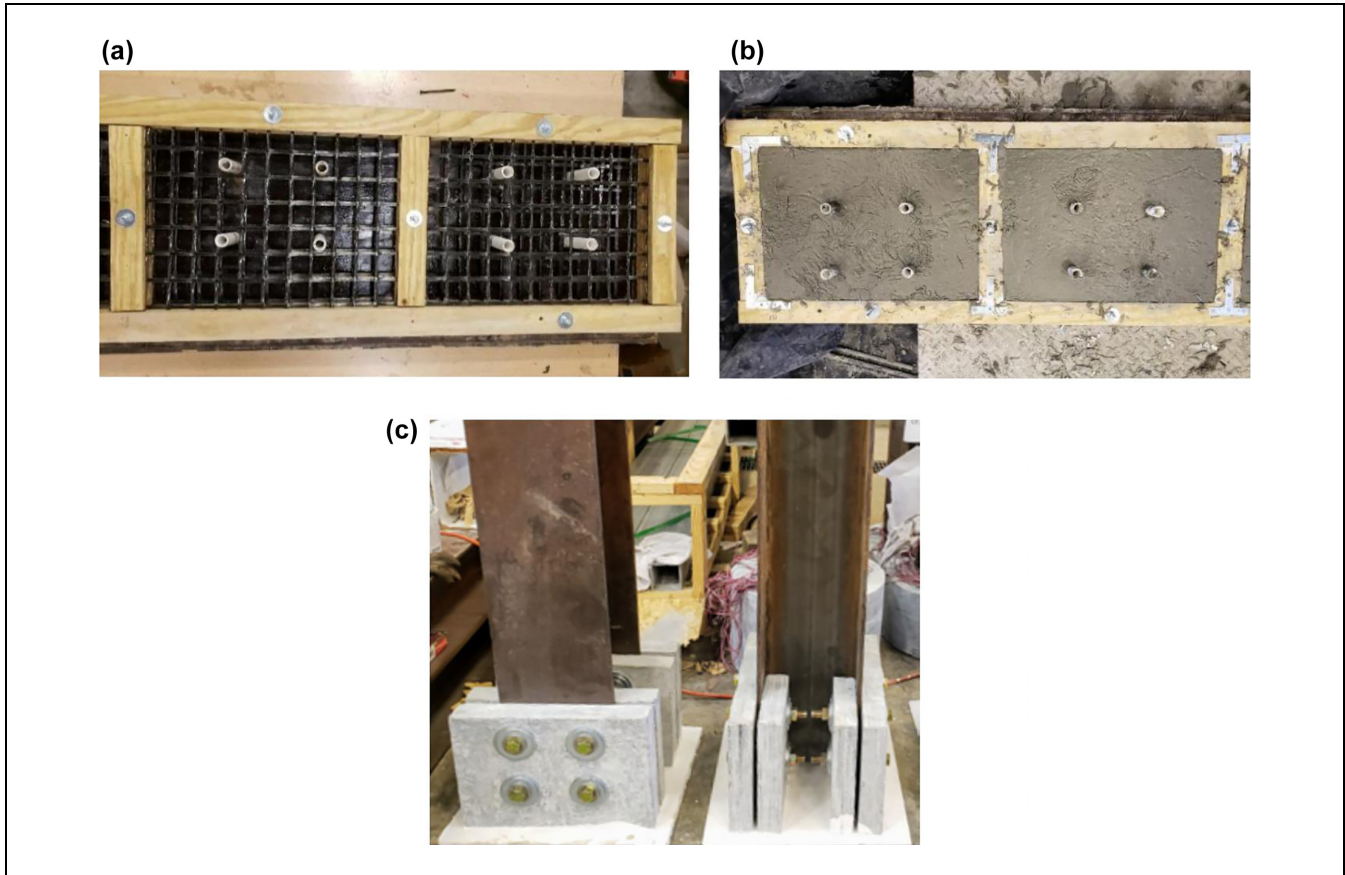


Figure 2. UHPC plates: (a) formwork with CFRP grids; (b) casting; and (c) bolted to a steel H-pile.
 Note: UHPC = ultrahigh-performance concrete; CFRP = carbon fiber-reinforced polymer.

Casting and Curing of UHPC Plates. The formwork for the UHPC plates was prepared as shown in Figure 2a. The required dimensions of CFRP grids were cut, and their ends were embedded on the sides of the formwork. A cover thickness equal to one-half t_{UHPC} was maintained for UHPC plates with one CFRP grid layer, while a cover thickness of 0.5 in. (12.7 mm) was used for UHPC plates with two CFRP grid layers (Figure 1). In the case of four CFRP grid layers, every two CFRP grid layers were bundled together, and a concrete cover thickness of 0.5 in. (12.7 mm) was used.

The fresh UHPC mixture was placed in the formwork (Figure 2b) without tamping rods or mechanical vibrators. Twelve 3 × 6-in. (76.2 × 152.4-mm) cylinders and 12 × 2-in. (50.8 mm) cubes were cast. The UHPC plates, cylinders, and cubes were then covered with plastic sheets to prevent moisture loss. They were demolded after one day and cured under a steam curing regime at a temperature of about 158°F (70°C) for another 24 h. They were then transferred to a moisture curing room, having a relative humidity of 95 ± 5% and temperature of about 70°F (21°C), for 5 to 7 days. Three replicate cylinders and cubes were tested on 3, 5, and 7 days to monitor the

compressive strength, f'_c per ASTM C1856/C1856M (53), ASTM C109/C109M (54), respectively. The moisture curing was stopped once the target compressive strength of 17 ksi (117 MPa) was achieved.

UHPC compressive strength, f'_c per ASTM C1856/C1856M (53), ASTM C109/C109M (54) and splitting tensile strength, f'_t per ASTM C496-96 (55) were determined on the testing day, about 10 days after casting. The average f'_c and f'_t were 19.2 ksi (132 MPa) and 2.6 ksi (18 MPa), with standard deviations of 0.32 and 0.14, respectively.

Specimen Fabrication. The UHPC plates were assembled on each flange of the steel H-piles using HSBC and heavy-hex nuts such that a clear edge distance between the bottom end of each steel H-pile and the bottom end of each UHPC plate was 2 in. (50.8 mm) (the distance c in Figure 1a). This edge distance allowed the steel H-pile to slip against the UHPC plates during testing. While assembling, a pretension load of 9,300 lb (41.4 kN) corresponding to 6.2% of the bolt's ultimate tensile strength was applied to each bolt to achieve a stable fixation

between the steel H-pile and the UHPC plates without causing any cracks on the UHPC plates.

Test Instrumentation and Set-Up

Each steel H-pile specimen with UHPC plates was subjected to push-out loading until failure occurred. The axial load was applied on the steel H-pile, which slipped against the attached UHPC plates. All specimens from Group A and two specimens from Group C, 0.75t-1D-1G and 1.5t-1D-1G, were tested using a 550 kips (2,446 kN) MTS universal testing machine (UTM) (Figure 3a and Table 1). The remaining specimens were tested using a 1,000 kips (4,450 kN) self-sustained testing frame (SSTF) (Figure 3b). The selected testing set-ups depended on the anticipated ultimate strength of the tested specimens.

For specimens tested in the UTM machine, each specimen was placed on a rigid steel base and aligned to the loading shaft to ensure concentric loading. A swivel plate was positioned on the top of the steel H-pile to uniformly transfer the load from the actuator to the steel H-pile (Figure 3a). This formed bottom-hinged and top-pin boundary conditions. A monotonic axial load at 0.05 in./min (1.27 mm/min) was applied to the top of the swivel plate.

For specimens tested using the SSTF, each specimen was placed between a movable and a fixed beam (Figure 3b). One end of the steel H-pile was inserted in a steel cap, connected with a half-sphere, and placed inside a swivel plate connected to the movable beam. The other end of the test specimen connected to the UHPC plates was supported on the fixed beam. This formed pin-hinge boundary conditions. The specimen was aligned in the horizontal and vertical planes to avoid eccentricity. Two hydraulic jacks, each with a capacity of 500 kips (2,225 kN), were inserted between the movable and fixed beams. The jacks were used to apply load at approximately 25 kips/min (110 kN/min) using an oil pump.

Two linear variable displacement transducers (LVDTs) were installed on each specimen to measure the relative axial displacement between the UHPC plates and the steel H-pile. In addition, for the SSTF set-up, two string potentiometers were attached between the movable and fixed beams along the length of each specimen to measure the overall displacement. A data acquisition system was used to collect the measurements at a frequency of 2 Hz.

Results and Discussion

Failure Modes and Axial Strengths

Figure 4 displays examples of the different failure modes of the test specimens being shearing-off of the HSBC, as

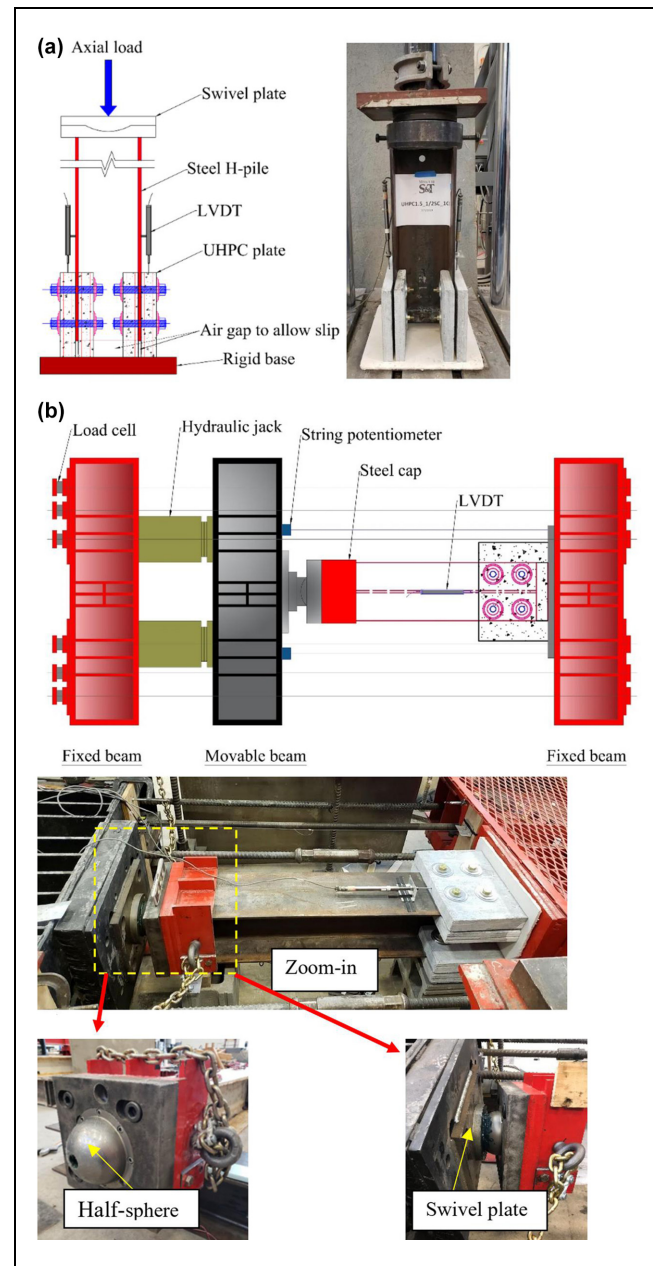


Figure 3. Specimens with instrumentation ready for testing in: (a) MTS universal testing machine (UTM); and (b) self-sustained testing frame (SSTF).

Note: UHPC = ultrahigh-performance concrete; LVDT = linear variable displacement transducers.

well as splitting and bearing failure of the UHPC plates with bolt bending yield. The arrows in the figure represent the push-out loading direction. The axial load versus the axial displacement is plotted in Figure 5. The axial load was obtained from the UTM load cell or sum of the loads recorded in the load cells installed on the post-tensioned bars of the SSTF, depending on the used test set-up. The axial displacement is calculated as the

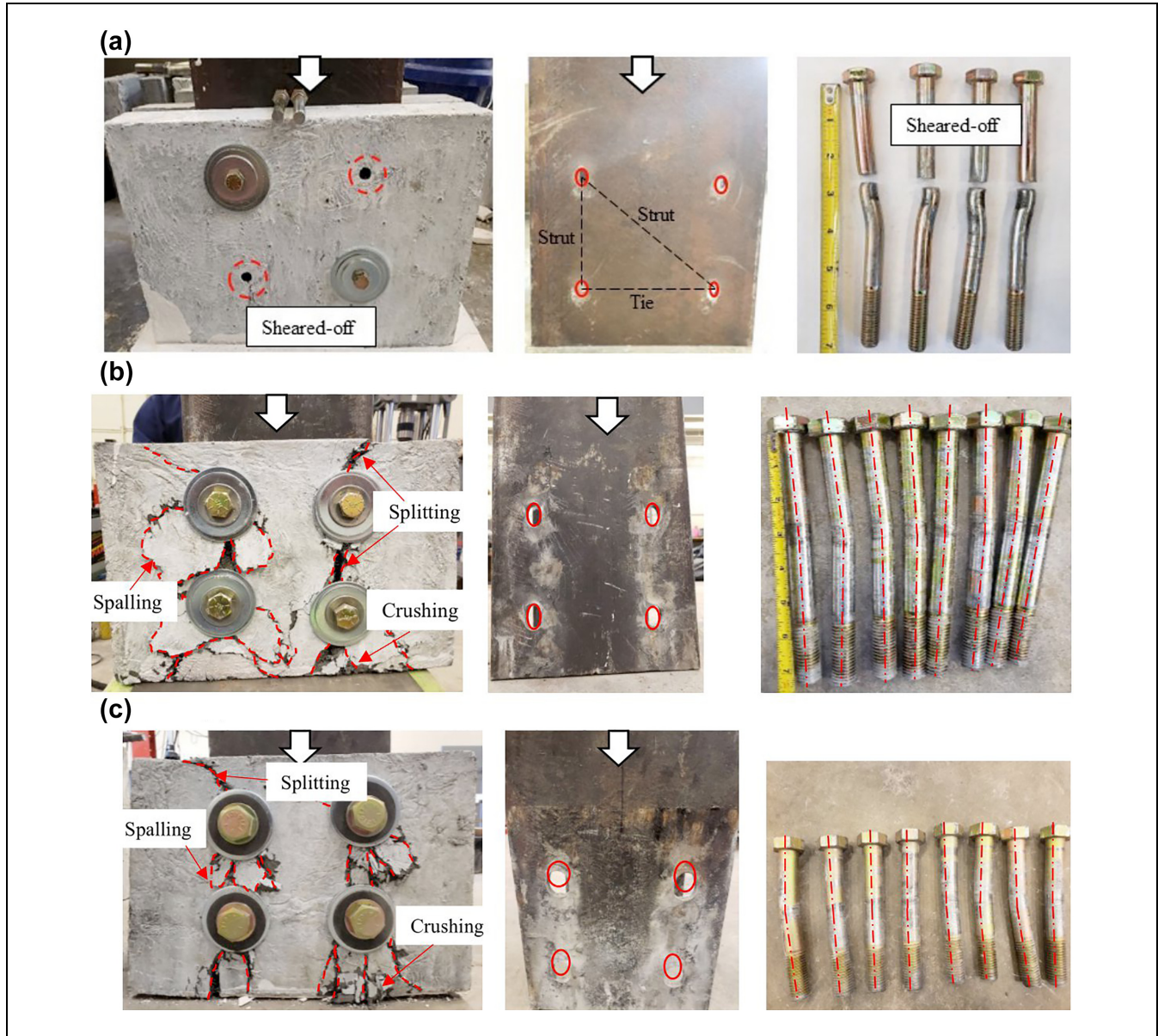


Figure 4. Typical failure modes for specimens having different HSBC diameters: (a) 2.25t-1/2D-1G; (b) 2.25t-3/4D-4G; and (c) 2.25t-1D-2G.

average values of the two LVDTs. The push-out test results and typical failure modes for each specimen are tabulated in Table 5, where the average bearing stress in the UHPC plates (σ_b), underneath the HSBC holes is defined using Equation 1.

$$\sigma_b = \frac{P_{max}}{nd_b t_{UHPC}} \quad (1)$$

where

P_{max} = peak load applied on the steel H-pile, kips (kN),

d_b = diameter of HSBC, in. (mm),

t_{UHPC} = thickness of UHPC plates, in. (mm), and

n = number of bearing surfaces = 16, that is, as four HSBCs connecting two UHPC plates in each flange of a steel H-pile.

Except for specimen 0.75t-1/2D-1G, which experienced UHPC bearing failure accompanied by HSBC yielding, all specimens with a 0.5-in. (12.7-mm) diameter HSBC displayed shearing-off of the HSBC with similar axial force versus displacement behavior (Figure 5a). Taking specimen 2.25t-1/2D-1G as an example, the typical mode of failure for specimens with a 0.5-in. (12.7-mm) diameter HSBC is shown in Figure 4a. Until an average load of approximately 8 kips (35 kN), no slipping was observed between the UHPC plates and the

Table 5. Push-Out Test Results

Specimen designation	Peak load (P_{max}) (kips [kN])	Displacement (δ_{max} *) (in. [mm])	P_{max}/P_o **	σ_b (ksi [MPa])	f'_c (ksi [MPa])***	Failure mode
A						
0.75t-1/2D-1G	219 (974)	0.41 (10.41)	0.35	18.25 (126)	18.6 (128)	UHPC bearing
1.5t-1/2D-1G	291 (1,292)	0.32 (8.08)	0.46	24.25 (167)	19.8 (137)	HSBC shear-off
2.25t-1/2D-1G	287 (1,277)	0.25 (6.35)	0.46	15.94 (110)	19.4 (134)	
2.25t-1/2D-2G	295 (1,312)	0.29 (7.37)	0.47	16.4 (113)	19.7 (136)	
B						
2.25t-3/4D-1G	502 (2,233)	0.49 (12.34)	0.8	18.6 (128)	19.1 (132)	UHPC splitting /bearing
2.25t-3/4D-2G	536 (2,384)	0.52 (13.21)	0.85	19.9 (137)	19.4 (134)	
2.25t-3/4D-4G	506 (2,251)	0.53 (13.46)	0.8	18.7 (129)	19.2 (132)	
C						
0.75t-1D-1G	279 (1,241)	0.15 (3.84)	0.44	23.25 (160)	19.5 (134)	UHPC splitting /bearing
1.5t-1D-1G	542 (2,411)	0.31 (7.87)	0.86	22.6 (156)	19.2 (132)	
2.25t-1D-1G	615 (2,736)	0.35 (8.89)	0.98	17.1 (118)	18.2 (125)	
2.25t-1D-2G	605 (2,691)	0.39 (9.90)	0.96	16.8 (116)	18.7 (129)	

Note: UHPC = ultrahigh-performance concrete; HSBC = high-strength bolt connectors; ksi = kips per square inch.

* At peak load.

** P_o Ultimate axial capacity of uncorroded steel H-pile = 630 kips (2,802 kN).

*** f'_c UHPC compressive strength at the testing day.

steel H-pile as a result of the pretension of the HSBCs and the mechanical friction along the steel-UHPC interface. As the interface mechanical friction was overcome at about 11 kips (49 kN), a slip occurred, and the HSBCs began to bear against the perimeters of the holes in the UHPC plates. With continuous loading to about 70% of P_{max} , the HSBCs started to yield resulting in a reduced slope of the axial force versus displacement curve (Figure 5a). The curve maintained the overall ascending trend until the specimen reached its peak axial load. The average peak load of the three test specimens, P_{max} , was about 291 kips (1,292 kN), corresponding to about 46% of the ultimate axial capacity (P_o) of the steel H-pile, at an axial displacement of about 0.28 in. (7.28 mm). It was followed by the shearing-off of two HSBCs in each flange (Figure 4a), one top and one bottom in a diagonal arrangement. This resulted in a stepwise drop in the axial strength of about 18% of P_{max} followed by 52% of P_{max} . This diagonal shearing-off is attributed to the redistribution of applied load among the remaining HSBCs after the shearing-off of the top HSBC, forming a strut and tie (Figure 4a), which in turn induced the maximum force in the bottom HSBC. The failure surface was on the shank of HSBC. Minor deformation of the holes in the steel H-pile was observed, however no damage was observed in the UHPC plates. It is worth noting that the average bearing stress (σ_b) in the UHPC plates underneath the HSBC for the specimens 2.25t-1/2D-1G and 2.25t-1/2D-2G was 17.5% lower than the unconfined compressive strength of the plates (f'_c), confirming that the failure of the specimens was not a result of the failure of the UHPC plates but rather the yielding and

shearing-off of the HSBC. For the specimen 1.5t-1/2D-1G, the bearing stress was 22% higher than f'_c . However, inspecting the tested specimen still indicated that failure occurred as a result of HSBC failure.

For Group B, the failure mode of specimens with a 0.75-in. (19-mm) diameter HSBC was UHPC splitting and bearing failure with yielding of the HSBC in bending. Figure 4b shows the failure mode of specimen 2.25t-3/4D-4G as an example. No slipping was observed in those specimens until an average load of 6 kips (27 kN), which was lower than that observed in the case of specimens with a 0.5-in. (12.7-mm) diameter HSBC. As the applied load was increased to approximately 9 kips (40 kN), the interfacial friction was overcome, and a slip occurred with HSBC bearing against the perimeter of the holes in the UHPC plates. With increasing the load to 64% to 70% of P_{max} , a decreasing slope of the axial force versus displacement curve was observed (Figure 5b). The reduced slope resulted from the development of vertical and diagonal cracks in the UHPC plates underneath the HSBC, near to the loading end, followed by bending of the HSBC. Because of bearing stress induced by the HSBC, crushing and splitting of the UHPC occurred resulting in spalling of the UHPC. The specimens reached P_{max} ranging from 502 kips (2,233 kN) to 536 kips (2,384 kN), corresponding to 79.7% to 85% of P_o , at an axial displacement ranging from 0.49 in. (12.34 mm) to 0.53 in. (13.46 mm) depending on the provided number of CFRP layers. With additional loading, the formed cracks extended along the entire length of the UHPC plates along with bending deformation in the HSBC. The average bearing stress in the UHPC plates

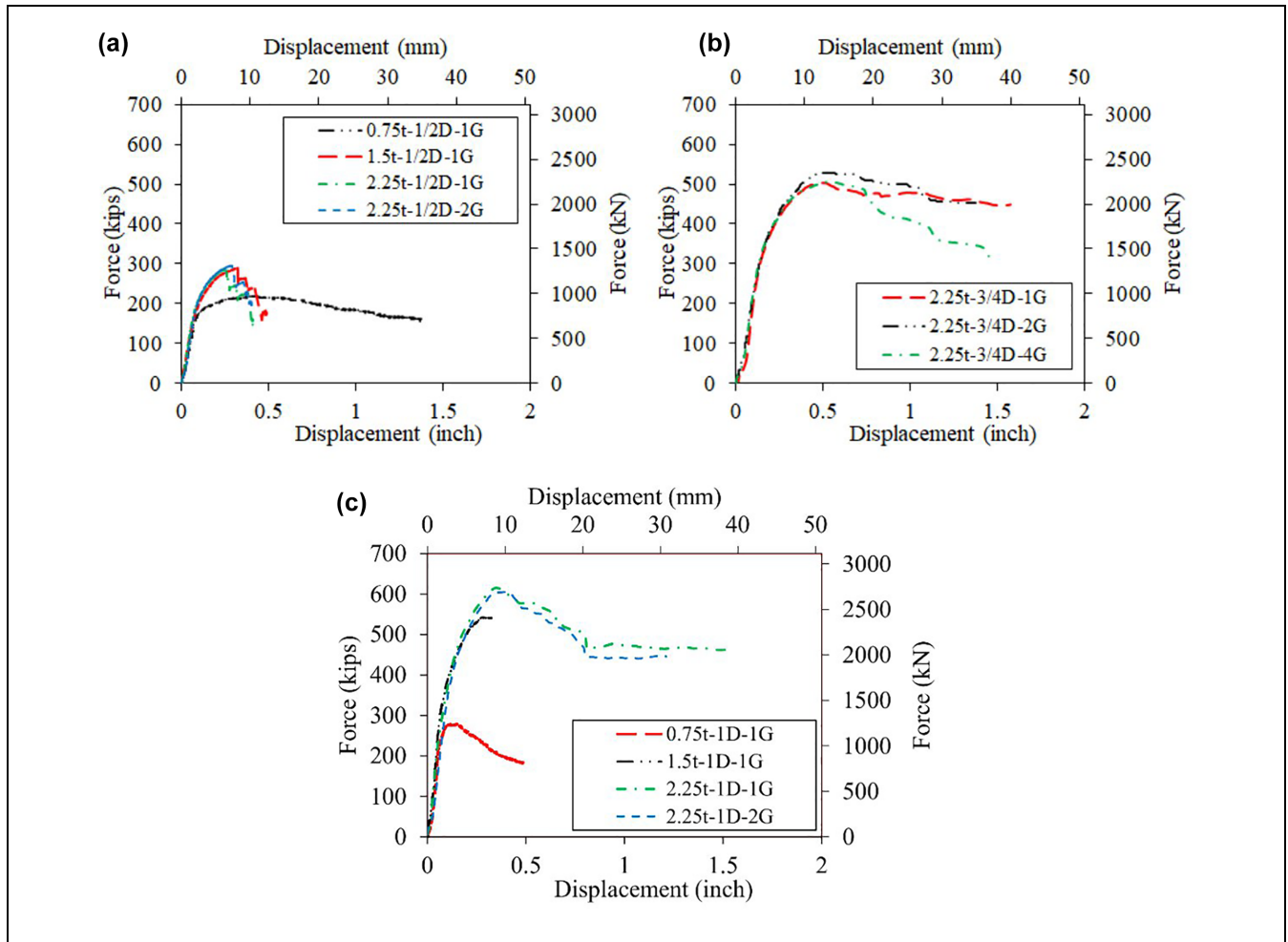


Figure 5. Force versus displacement of the push-out specimens: (a) Group A; (b) Group B; and (c) Group C.

underneath the HSBC reached approximately 99% of f'_c . The HSBC holes in the steel H-piles elongated as well (Figure 4b).

For Group C, the failure mode of specimens with a 1-in. (25.4-mm) diameter HSBC (Figure 4c) was similar to that of specimens having a 0.75-in. (19-mm) diameter HSBC, that is, UHPC splitting and bearing failure with yielding the HSBC in bending. Figure 5b shows the failure mode of specimen 2.25t-1D-2G as an example for this group. Up to an average load of approximately 12.5 kips (55.6 kN), slipping between the UHPC and steel was not observed. Once the friction between the UHPC plates and steel pile was overcome, a slip occurred, causing the HSBC to bear against the surfaces of the holes in the UHPC plates. As the average load was increased to approximately 83% to 89% of P_{max} , cracks developed in the UHPC plates underneath the lower HSBC. This corresponded to the decreased slope of the axial force versus displacement curve (Figure 5c). The specimens reached P_{max} ranging from 1,241 kips (279 kN) to 2,736 kips

(615 kN), corresponding to 44% to 98% of P_o , at displacements ranging from 0.15 in. (3.8 mm) to 0.39 in. (9.9 mm), respectively. Loading beyond P_{max} led to the crushing of UHPC plates underneath the HSBC and widening of the splitting cracks extending through the plates and bending of the HSBCs (Figure 4c). The average bearing stress in the UHPC plates underneath the HSBC was about 105% of the average f'_c . The holes in the steel H-piles deformed in an oval shape.

Influence of the Investigated Parameters on Axial Load

Two groups of specimens having t_{UHPC} of 2.25 in. (57 mm) and either one or two layers of CFRP grids. Each group included a 0.5-in. (12.7-mm), 0.75-in. (19-mm), or 1-in. (25.4-mm) diameter HSBC to determine the effects of HSBC diameter on the axial load capacity (Figure 6a). Increasing the diameter of the HSBC increased the axial load capacity of the investigated specimens with an insignificant effect of the number of

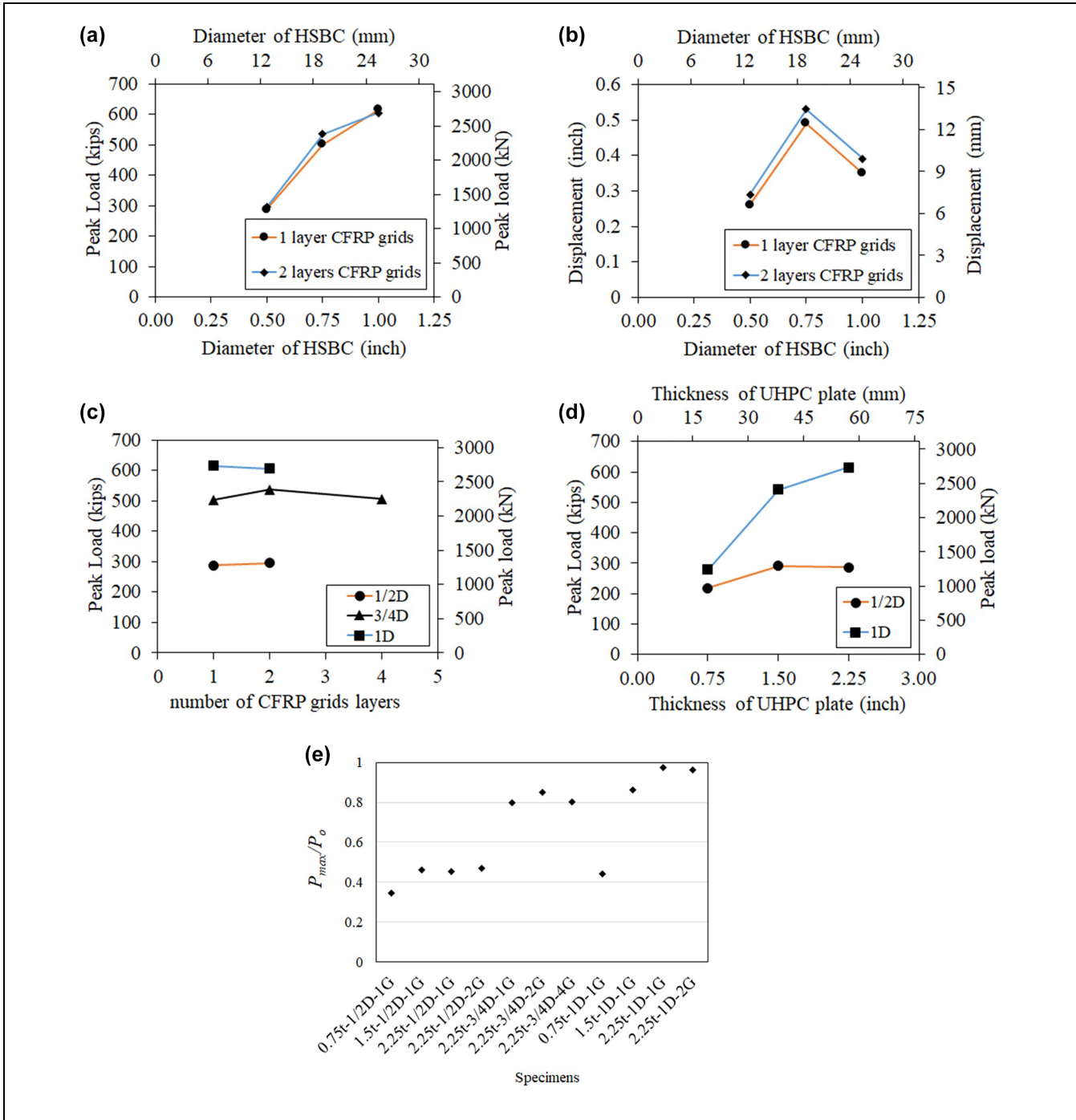


Figure 6. (a–b) Effect of diameter of HSBC; (c) effect of number of layers of CFRP grids; (d) effect of thickness of UHPC plate; and (e) P_{max} of all test specimens normalized by P_o .
 Note: UHPC = ultrahigh-performance concrete; HSBC = high-strength bolt connectors; CFRP = carbon fiber-reinforced polymer.

CFRP layers (Table 5 and Figure 6a). The rate of strength increased was nonlinear as a result of the change in the mode of failure with changing the HSBC diameter. Increasing the HSBC diameter from 0.5 in. (12.7 mm) to 0.75 in. (19 mm) and 25.4 mm (1 in.), corresponding to

increasing the cross-sectional area by 125% and 300%, displayed an average of 77.5% and 109.5% higher P_{max} , respectively. Changing the HSBC diameter changed the failure mode from HSBC shear-off in the specimens with a 0.5-in. (12.7-mm) diameter to UHPC splitting and

bearing failure in the remaining specimens. The displacement at the peak load for the specimens with a 0.50-in. (12.7-mm) diameter HSBCs was approximately 0.28 in. (7 mm) (Figure 6b), while those with a 0.75-in. (19-mm) and a 1-in. (25.4-mm) diameter HSBCs displayed displacements of approximately 0.51 in. (13 mm) and 0.37 in. (9.4 mm), respectively (Figure 6b). The change in the displacement linked to the change in the mode of failure from the shear-off of the 0.50-in. (12.7-mm) diameter HSBCs to UHPC splitting and bearing for specimens having a 0.75-in. (19-mm) and 1-in. (25.4-mm) diameter HSBCs.

Figure 6c shows the effect of CFRP grid layers on the axial load. Two groups of specimens with a 0.5-in. (12.7-mm), or 1-in. (25.4-mm) diameter HSBCs with one and two CFRP grid layers were investigated. A third group had a 0.75-in. (19-mm) diameter HSBC with one, two, or four CFRP grid layers was also investigated. All specimens had t_{UHPC} of 2.25 in. (57 mm). The axial load of the test specimens largely remained the same with changing the number of CFRP grid layers. When the number of CFRP grid layers was increased from single to double layers, P_{max} changed by an average of 2.47%. Furthermore, increasing the CFRP grid layers from two to four while having a 0.75-in. (19-mm) diameter HSBC decreased P_{max} by 5.6%.

Figure 6d shows the effect of the t_{UHPC} on the axial load. Two groups of specimens, each group including three specimens with one layer of CFRP grid and having different t_{UHPC} of 0.75 in. (19 mm), 1.5 in. (38.1 mm), and 2.25 in. (57 mm), were investigated. The first group had a 0.5-in. (12.7-mm) diameter HSBC, while the second had a 1-in. (25.4-mm) diameter HSBC. Increasing the t_{UHPC} changed the P_{max} nonlinearly. In the case of specimens having a 0.5-in. (12.7-mm) diameter HSBC, increasing the t_{UHPC} from 0.75 in. (19 mm) to 1.5 in. (38.1 mm) increased P_{max} by 33%. Beyond that, increasing t_{UHPC} did not change P_{max} since the dominant mode of failure was HSBC shearing-off. In the case of specimens having a 1-in. (25.4-mm) diameter HSBC, increasing the t_{UHPC} from 0.75 in. (19 mm) to 1.5 in. (38.1 mm) and 2.25 in. (57 mm) increased P_{max} by 95% and 14%, respectively. The dominant failure mode in this group of specimens was UHPC splitting and bearing. Therefore, increasing t_{UHPC} increased the specimens' strengths.

Figure 6e displays P_{max} of each tested specimen normalized by P_o (strength of the uncorroded steel H-pile). A normalized strength value of 1.0 indicates that the UHPC connection could transfer 100% of the ultimate axial strength of the steel H-pile. The normalized strength of the test specimens ranged from 35% to 98%, depending on the HSBC diameter and t_{UHPC} . Specimens having HSBC diameter of 1 in. (25.4 mm) and t_{UHPC} of 2.25 in. (57 mm), that is, 2.25t-1D-1G and 2.25t-1D-2G, could

transfer an average 97% P_o . However, it was not the case for specimens with a 1-in. (25.4-mm) diameter HSBC and t_{UHPC} less than 2.25 in. (57 mm). Small t_{UHPC} led to crushing and splitting of the UHPC plates before the HSBC yielding, resulting in smaller ultimate strength compared with 2.25t-1D-1G and 2.25t-1D-2G. For other specimens with HSBC diameters of 0.5 in. (12.7 mm) and 0.75 in. (19 mm), the normalized strength ranged from 35% to 47% and from 80% to 85%, respectively.

Evaluation of Test Results

The axial force applied to the steel H-piles during the push-out test transferred through the HSBCs in the form of shear force to the UHPC plates. There is no established equation to predict the shear strength of post-installed anchors in UHPC; therefore, the shear strength equations for post-installed anchors and cast-in headed stud shear connectors in normal-strength concrete were used to calculate the shear strength of the tested specimens. While these equations may not provide an exact estimation of the shear strength of HSBCs in UHPC, they serve as a useful initial assessment to evaluate their performance.

Design codes such as AISC (56), AASHTO LRFD (47), ACI 318 (48) and Eurocode-4 (57) provide equations based on the failure mode to compute the shear strength of shear studs embedded in normal-strength concrete. The ultimate HSBC shear strength, V_s for cast-in-place anchor, according to AISC (I8-3), AASHTO LRFD (Equation 6.10.10.4.3.1), and ACI (Equation 17.7.1.2a) can be calculated using Equation 2.

$$V_s = A_s f_u \quad (2)$$

where A_s is cross-sectional area of HSBC and f_u is specified minimum tensile strength of an HSBC.

Eurocode-4 (Equation 6.18) suggests a 0.8 reduction factor to Equation 1 to calculate the V_s (Equation 3):

$$V_s = 0.8 A_s f_u \quad (3)$$

For post-installed anchor, the ultimate HSBC shear strength, V_s , based on Equation 17.7.1.2b in the ACI is given by Equation 4.

$$V_s = 0.6 A_s f_u \quad (4)$$

For concrete failure, both the AISC (I8-1) and AASHTO LRFD (Equation 6.10.10.4.3.1) recommend the same equation to calculate the ultimate shear strength (V_c) (Equation 5):

$$V_c = 0.5 A_s \sqrt{f'_c E_c} \quad (5)$$

$$E_c = 46200 \sqrt{f'_c}, psi \quad (6)$$

Table 6. Comparison of Predicted and Experimental Strength

Specimen designation	Experimental(P_{max} [kips])	AISC, AASHTO		Eurocode-4		ACI 318		
		V_s (kips)	V_c (kips)	V_s (kips)	V_c (kips)	V_s (kips)	V_{cb} (kips)	V_{cp} (kips)
0.75t-1/2D-1G	219	471	546	377	161	283	34	49
1.5t-1/2D-1G	291	471	551	377	203	283	49	140
2.25t-1/2D-1G	287	471	555	377	205	283	59	178
2.25t-1/2D-2G	295	471	557	377	206	283	59	178
2.25t-3/4D-1G	502	1,060	1,254	848	463	636	67	178
2.25t-3/4D-2G	536	1,060	1,249	848	461	636	67	178
2.25t-3/4D-4G	506	1,060	1,249	848	461	636	67	178
0.75t-1D-1G	279	1,885	2,186	1,508	404	1,131	42	49
1.5t-1D-1G	542	1,885	2,203	1,508	651	1,131	60	140
2.25t-1D-1G	615	1,885	2,220	1,508	820	1,131	73	178
2.25t-1D-2G	605	1,885	2,246	1,508	829	1,131	73	178

Note: AISC = American Institute of Steel Construction; 1 kip = 4.448 kN.

where f'_c is unconfined compressive strength of concrete and E_c is the modulus of elasticity of concrete.

The ultimate shear strength for concrete failure provided by Eurocode-4 (Equation 6.19) is given in Equation 7.

$$V_c = 0.29\alpha d^2 \sqrt{f'_c E_c} \quad (7)$$

where α is the factor considering the height-to-diameter ratio of a bolt and is calculated as $\alpha = 0.2(\frac{h}{d} + 1) \leq 1$, where d and h are the diameter and the embedment length of the HSBC, i.e., the sum of the thickness of the flange of the steel H-pile and the thickness of the two UHPC plates, respectively.

Equation 17.7.2.1b of the ACI 318 provides the ultimate shear strength for concrete failure in the form of concrete breakout or pryout strength in shear. For an anchor group, the breakout strength is given as V_{cb} per Equation 8 (ACI).

$$V_{cb} = \frac{A_{Vc}}{A_{Vco}} \psi_{ec} \psi_{ed} \psi_c \psi_h V_b \quad (8)$$

where $\frac{A_{Vc}}{A_{Vco}}$, ψ_{ec} , ψ_{ed} , ψ_c , and ψ_h are reduction factors accounting for the projected area of failure surface, eccentricity, edge effects, cracking, and small concrete depth, respectively, and V_b is the basic concrete breakout strength of a single anchor in shear (Equation 17.7.2.2.1) and can be calculated as the smaller of Equations 9 and 10.

$$V_b = 7 \left(\frac{l_e}{d} \right)^{0.2} \sqrt{d} \lambda_a \sqrt{f'_c} (C_{a1})^{1.5} \quad (9)$$

$$V_b = 9 \lambda_a \sqrt{f'_c} (C_{a1})^{1.5} \quad (10)$$

where

l_e is the load-bearing length of the anchor for shear,

λ_a is the modification factor to reflect the reduced mechanical properties of lightweight concrete, and C_{a1} is the edge distance to the near edge anchor.

For an anchor group, the pryout strength is given as V_{cp} as in Equation 11 (ACI 17.7.3.1b).

$$V_{cp} = k_{cp} \frac{A_{Nc}}{A_{Nco}} \psi_{ec} \psi_{ed} \psi_c \psi_{cp} N_b \quad (11)$$

where

$\frac{A_{Nc}}{A_{Nco}}$, ψ_{ec} , ψ_{ed} , ψ_c , and ψ_h are reduction factors accounted for the projected area of failure surface, eccentricity, edge effects, cracking, and splitting factor, respectively, k_{cp} is coefficient of pryout strength, and N_b is the basic concrete breakout strength of a single anchor in tension (Equation 17.6.2.2.1) and is given by Equation 12.

$$N_b = k_c \lambda_a \sqrt{f'_c} (h_{ef})^{1.5} \quad (12)$$

where k_c is the coefficient of basic concrete breakout strength in tension and h_{ef} is the effective embedment depth of the anchor.

Table 6 compares the experimental strengths with those predicted using Equations 2 through 12.

Figure 7 represents comparative graphs of the ultimate strength predicted from the models and the corresponding experimental results for different modes of failure. For specimens failed because of shear-off mode (Table 5), Equations 2 and 3 both over-predicted V_s compared with the experimental results, with an average V_s/P_{max} of 1.62 and 1.30 respectively (Figure 7a). Equation 4 ACI 318, however, closely predicted V_s , with an average V_s/P_{max} of 0.97 (Figure 7a). This is anticipated since Equations 2 and 3 developed for the cast-in-place anchor, whereas Equation 4 was developed for the post-installed anchor. For the concrete failure mode,

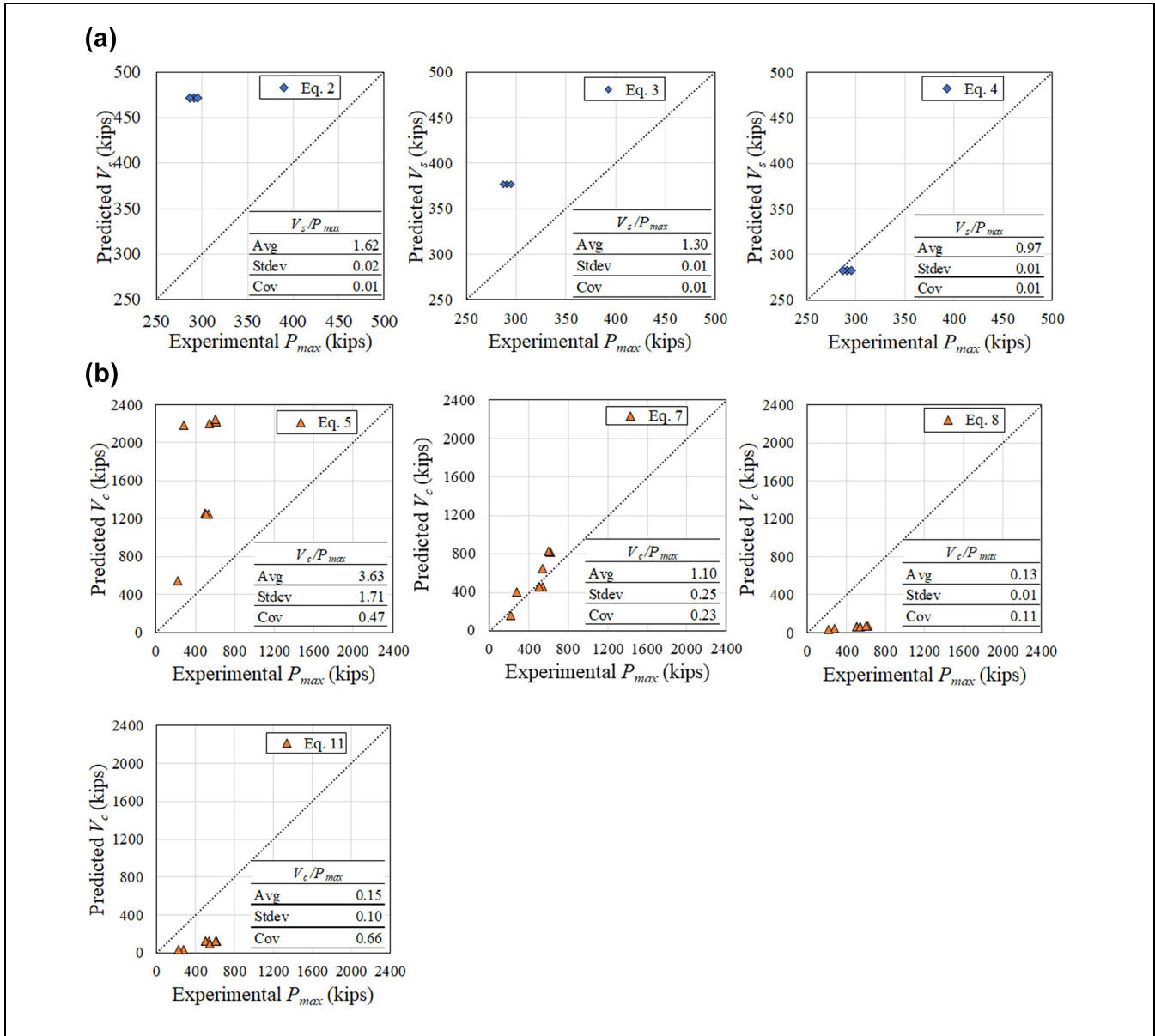


Figure 7. Comparisons of ultimate strength between experimental results and current design codes for: (a) shear-off failure mode; and (b) concrete failure mode.

Equation 5 over-predicted V_c , while Equations 8 and 11 under-predicted V_c compared with the experimental results, with average V_c/P_{max} to be 3.63, 0.13, and 0.21 respectively (Figure 7b). Equation 7, however, displayed a good correlation with the experimental results, with an average V_c/P_{max} to be 1.1 (Figure 7b).

Conclusions

This paper presents a rapid repair method using ultrahigh-performance concrete (UHPC) plates. The plates encase the flanges of a steel H-pile along the corroded segment

and extend beyond that to the uncorroded sections, where high-strength bolt connectors (HSBCs) attach the plates to the steel pile. Eleven push-out tests were conducted in this study to investigate the behavior of the steel H-pile encased with the UHPC plates. The effects of the UHPC plate thickness, the diameter of high-strength bolt connector (HSBC), and the number of layers of carbon fiber-reinforced polymer (CFRP) grids were investigated. The UHPC plates attached to the steel H-pile could transfer axial loads ranging from 35% to 98% of the steel H-piles ultimate axial capacity. The experimental work led to the following findings and conclusions:

1. The peak axial load of the test specimens did not change with changing the number of CFRP grid layers.
2. Increasing the diameter of the HSBC increased the axial load capacity (P_{max}) and changed the failure mode of the investigated specimens. Changing the diameter from 0.5 in. (12.7 mm) to 0.75 in. (19 mm) and to 1 in. (25.4 mm) changed the mode of failure from shear-off of the HSBCs in the case of the specimens 2.25t-1/2D-1G and 2.25t-1/2D-2G to UHPC splitting and crushing in the remaining specimens. The change in the diameter resulted in an average of 77.5% and 109.5% increase in the strength of the test specimens, respectively.
3. Increasing the t_{UHPC} changed the specimens' axial loads nonlinearly. In the case of specimens having a 0.5-in. (12.7-mm) diameter HSBC, increasing the t_{UHPC} from 0.75 in. (19 mm) to 1.5 in. (38.1 mm) increased P_{max} by 33%. Beyond that increasing t_{UHPC} did not change P_{max} since the dominant mode of failure was HSBC shearing-off. In the case of specimens having a 1-in. (25.4-mm) diameter HSBC, increasing the t_{UHPC} from 0.75 in. (19 mm) to 1.5 in. (38.1 mm) and 2.25 in. (57 mm) increased P_{max} by 95% and 14%, respectively. The dominant failure mode in this group of specimens was UHPC splitting and bearing. Therefore, increasing t_{UHPC} increased the specimens' strength.
4. For HSBC shear-off failure mode, the code equations according to AISC, AASHTO LRFD, and Eurocode-4 over-predicted the ultimate shear strength compared with the experimental results. In contrast, Equation 4 as per ACI 318 more accurately predicted the ultimate shear strength.
5. For concrete failure mode, the code equations according to AISC, AASHTO LRFD over-predicted the ultimate shear strength, whereas it was underpredicted as per ACI 318 compared with the experimental results. On the other hand, Eurocode-4 was observed to have a good correlation with the experimental results, with an average V_c/P_{max} to be 1.1.

Author Contributions

The authors confirm the contribution to the paper as follows: study conception and design: M. ElGawady; data collection: B. Shrestha; analysis and interpretation of results: B. Shrestha M. Abdulazeez, A. Ghani, and M. ElGawady; draft manuscript preparation: B. Shrestha; editing and reviewing the manuscript: A. Ghani, M. Abdulazeez, and M. ElGawady. All authors reviewed the results and approved the final version of the manuscript.


Declaration of Conflicting Interests


The author(s) declared no potential conflicts of interest with respect to the research, authorship, and/or publication of this article.

Funding

The author(s) disclosed receipt of the following financial support for the research, authorship, and/or publication of this article: This research project was funded by Mid-America Transportation Center (MATC) and Missouri Department of Transportation (MoDOT). It was conducted in the High-bay Structural Laboratory of Missouri University of Science and Technology.

ORCID iDs

Binod Shrestha  <https://orcid.org/0000-0002-0654-5867>

Ahmed Ghani  <https://orcid.org/0000-0001-9042-869X>

Mohanad M. Abdulazeez  <https://orcid.org/0000-0003-4641-9803>

Mohamed A. ElGawady  <https://orcid.org/0000-0001-6928-9875>

References

1. Karagah, H., C. Shi, M. Dawood, and A. Belarbi. Experimental Investigation of Short Steel Columns with Localized Corrosion. *Thin-Walled Structures*, Vol. 87, 2015, pp. 191–199.
2. Ramadan, A., and M. ElGawady. Axial Behavior of Corroded H-Piles. *Proc., IABSE 8 Congress*, No. 9, New York City, NY, International Association for Bridge and Structural Engineering (IABSE), September 4–6, 2019.
3. Shi, C., H. Karagah, M. Dawood, and A. Belarbi. Numerical Investigation of H-Shaped Short Steel Piles with Localized Severe Corrosion. *Engineering Structures*, Vol. 73, 2014, pp. 114–124.
4. Abdulazeez, M., B. Shrestha, E. Gomaa, A. Ramadan, and M. A. ElGawady. Bond Behavior of Steel H-Pile Bridge Columns Encased in Concrete Jackets. Presented at Transportation Research Board, Washington, D.C., 2019.
5. Abdulazeez, M. M., B. Shrestha, and M. A. ElGawady. Retrofit of Corroded Steel H-Piles Using Concrete Encased in CFRP. Presented at 10th New York City Bridge Conference, New York City, NY, 2019.
6. Karagah, H., M. Dawood, and A. Belarbi. Experimental Study of Full-Scale Corroded Steel Bridge Piles Repaired Underwater with Grout-Filled Fiber-Reinforced Polymer Jackets. *Journal of Composites for Construction*, Vol. 22, No. 3, 2018, p. 04018008.
7. Liu, X., A. Nanni, P. F. Silva, and R. A. Laboube. Rehabilitation of Steel Bridge Columns with FRP Composite Materials. *Proc. CCC, Composites in Construction*, Porto, Portugal, October 10–12, 2001. pp. 613–617.
8. de Larrard, F., and T. Sedran. Optimization of Ultra-High-Performance Concrete by the Use of a Packing Model. *Cement and Concrete Research*, Vol. 24, No. 6, 1994, pp. 997–1009.

9. Graybeal, B. *Ultra-High Performance Concrete*. Report No. FHWA-HRT-11-038. Federal Highway Administration, Washington, D.C., 2011.
10. Perry, V. Ductal®-A Revolutionary New Material for New Solutions. Association of Professional Engineers and Geoscientists of the Province of Manitoba (APEGM). 2006. https://www.apegm.mb.ca/pdf/PD_Papers/ductal.pdf
11. Shafieifar, M., M. Farzad, and A. Azizinamini. Experimental and Numerical Study on Mechanical Properties of Ultra High Performance Concrete (UHPC). *Construction and Building Materials*, Vol. 156, 2017, pp. 402–411.
12. Wille, K., A. E. Naaman, and G. Parra-Montesinos. Ultra-High Performance Concrete with Compressive Strength Exceeding 150 MPa (22 ksi): A Simpler Way. *ACI Material Journal*, Vol. 108, No. 1, 2011, pp. 34–46.
13. Graybeal, B., and J. Tanesi. Durability of an Ultrahigh-Performance Concrete. *Journal of Materials in Civil Engineering*, Vol. 19, No. 10, 2007, pp. 848–854.
14. Burkart, I., and H. S. Müller. Creep and Shrinkage Characteristics of Ultra High Strength Concrete (UHPC). *Proc., Second International Symposium on Ultra High Performance Concrete*, Kassel University Press GmbH, Germany, 2008, pp. 469–476.
15. Wu, Z., C. Shi, W. He, and D. Wang. Static and Dynamic Compressive Properties of Ultra-High Performance Concrete (UHPC) with Hybrid Steel Fiber Reinforcements. *Cement and Concrete Composites*, Vol. 79, 2017, pp. 148–157.
16. Alkaysi, M., and S. El-Tawil. Effects of Variations in the Mix Constituents of Ultra High Performance Concrete (UHPC) on Cost and Performance. *Materials and Structures*, Vol. 49, No. 10, 2016, pp. 4185–4200.
17. Banerji, S., and V. Kodur. Effect of Temperature on Mechanical Properties of Ultra-High Performance Concrete. *Fire and Materials*, Vol. 46, No. 1, 2022, pp. 287–301.
18. Graybeal, B. A. *Material Property Characterization of Ultra-High Performance Concrete*. No. FHWA-HRT-06-103. United States. Federal Highway Administration. Office of Infrastructure Research and Development, McLean, VA, 2006.
19. Tai, Y.-S., S. El-Tawil, B. Meng, and W. Hansen. Parameters Influencing Fluidity of UHPC and Their Effect on Mechanical and Durability Properties. *Journal of Materials in Civil Engineering*, Vol. 32, No. 10, 2020, p. 04020298.
20. Ichikawa, S., H. Matsuzaki, A. Moustafa, M. A. ElGawady, and K. Kawashima. Seismic-Resistant Bridge Columns with Ultrahigh-Performance Concrete Segments. *Journal of Bridge Engineering*, Vol. 21, No. 9, 2016, p. 04016049.
21. Farzad, M., M. Shafieifar, and A. Azizinamini. Accelerated Retrofitting of Bridge Elements Subjected to Predominantly Axial Load Using UHPC Shell. No. 18-05067. In *Proc., of the Transportation Research Board 97th Annual Meeting*, Washington, D.C., 2018.
22. Li, X., J. Wang, Y. Bao, and G. Chen. Cyclic Behavior of Damaged Reinforced Concrete Columns Repaired with High-Performance Fiber-Reinforced Cementitious Composite. *Engineering Structures*, Vol. 136, 2017, pp. 26–35.
23. Graybeal, B. A. Flexural Behavior of an Ultrahigh-Performance Concrete I-Girder. *Journal of Bridge Engineering*, Vol. 13, No. 6, 2008, pp. 602–610.
24. Steinberg, E. Structural Reliability of Prestressed UHPC Flexure Models for Bridge Girders. *Journal of Bridge Engineering*, Vol. 15, No. 1, 2010, pp. 65–72.
25. Sturm, A., P. Visintin, R. Seracino, G. Lucier, and D. Oehlers. Flexural Performance of Pretensioned Ultra-High Performance Fibre Reinforced Concrete Beams with CFRP Tendons. *Composite Structures*, Vol. 243, 2020, p. 112223.
26. Yoo, D.-Y., N. Banthia, and Y.-S. Yoon. Flexural Behavior of Ultra-High-Performance Fiber-Reinforced Concrete Beams Reinforced with GFRP and Steel Rebars. *Engineering Structures*, Vol. 111, 2016, pp. 246–262.
27. Yang, Y., J. Walraven, and J. Den Uijl. Study on Bending Behavior of an UHPC Overlay on a Steel Orthotropic Deck. *Proc., 2nd International Symposium on Ultra High Performance Concrete*, University of Kassel, Germany, 2008, pp. 639–646.
28. Hossain, K., L. R. Gladson, and M. S. Anwar. Modeling Shear Strength of Medium-to Ultra-High-Strength Steel Fiber-Reinforced Concrete Beams Using Artificial Neural Network. *Neural Computing and Applications*, Vol. 28, No. 1, 2017, pp. 1119–1130.
29. Hou, L.-j., Z.-y. Luan, D. Chen, and S.-l. Xu. Experimental Study of the Shear Properties of Reinforced Ultra-High Toughness Cementitious Composite Beams. *Journal of Zhejiang University-SCIENCE A*, Vol. 16, No. 4, 2015, pp. 251–264.
30. Lim, W.-Y., and S.-G. Hong. Shear Tests for Ultra-High Performance Fiber Reinforced Concrete (UHPFRC) Beams with Shear Reinforcement. *International Journal of Concrete Structures and Materials*, Vol. 10, No. 2, 2016, pp. 177–188.
31. Mészöly, T., and N. Randl. Shear Behavior of Fiber-Reinforced Ultra-High Performance Concrete Beams. *Engineering Structures*, Vol. 168, 2018, pp. 119–127.
32. Schramm, N., and O. Fischer. Investigations on the Shear Behavior of Bridge Girders Made of Normal and Ultra-High Performance Fiber-Reinforced Concrete. *Procedia Engineering*, Vol. 156, 2016, pp. 411–418.
33. Voo, Y. L., W. K. Poon, and S. J. Foster. Shear Strength of Steel Fiber-Reinforced Ultrahigh-Performance Concrete Beams Without Stirrups. *Journal of Structural Engineering*, Vol. 136, No. 11, 2010, pp. 1393–1400.
34. Yang, I.-H., C. Joh, J. W. Lee, and B.-S. Kim. Torsional Behavior of Ultra-High Performance Concrete Squared Beams. *Engineering Structures*, Vol. 56, 2013, pp. 372–383.
35. McMullen, K. F., and A. E. Zaghi. Experimental Evaluation of Full-Scale Corroded Steel Plate Girders Repaired with UHPC. *Journal of Bridge Engineering*, Vol. 25, No. 4, 2020, p. 04020011.
36. Zmetra, K. M., K. F. McMullen, A. E. Zaghi, and K. Wille. Experimental Study of UHPC Repair for Corrosion-Damaged Steel Girder Ends. *Journal of Bridge Engineering*, Vol. 22, No. 8, 2017, p. 04017037.
37. Shrestha, B., A. Ghani, M. M. Abdulazeez, and M. A. ElGawady. Innovative Approach to Repair Corroded Steel Piles Using Ultra-High Performance Concrete. *Transportation Research Record: Journal of the Transportation Research Board*, 2020. 2674: 1–14.

38. Tomek, R. Advantages of Precast Concrete in Highway Infrastructure Construction. *Procedia Engineering*, Vol. 196, 2017, pp. 176–180.
39. Yee, A. A., and P. H. D. Eng. Social and Environmental Benefits of Precast Concrete Technology. *PCI Journal*, Vol. 46, No. 3, 2001, pp. 14–19.
40. Abdulazeez, M. M., A. Ramadan, B. Sherstha, A. Ghenni, E. Gomaa, Y. Darwish, and M. A. ElGawady. *Behavior and Repair of Corroded Steel H-Piles Phase I (Axial Behavior)*. No. 25-1121-0005-133-1. Mid-America Transportation Center, Lincoln, NE, 2019.
41. Abdulazeez, M. M., A. Ramadan, B. Shrestha, E. Gomaa, T. Mahmood, A. Ghenni, and M. A. ElGawady. *Behavior and Repair of Corroded Steel H-Piles*. No. cmr 21-002. Missouri. Department of Transportation. Construction and Materials Division, U. S. Department of Transportation, Federal Highway Administration, Washington, D.C., 2021. <https://rosap.ntl.bts.gov/view/dot/56945>.
42. Fang, Z., W. Liang, H. Fang, H. Jiang, and S. Wang. Experimental Investigation on Shear Behavior of High-Strength Friction-Grip Bolt Shear Connectors in Steel-Precast UHPC Composite Structures Subjected to Static Loading. *Engineering Structures*, Vol. 244, 2021, p. 112777.
43. Wang, J., J. Qi, T. Tong, Q. Xu, and H. Xiu. Static Behavior of Large Stud Shear Connectors in Steel-UHPC Composite Structures. *Engineering Structures*, Vol. 178, 2019, pp. 534–542.
44. Zhang, Y., B. Chen, A. Liu, Y.-l. Pi, J. Zhang, Y. Wang, and L. Zhong. Experimental Study on Shear Behavior of High Strength Bolt Connection in Prefabricated Steel-Concrete Composite Beam. *Composites Part B: Engineering*, Vol. 159, 2019, pp. 481–489.
45. Zhang, Y., A. Liu, B. Chen, J. Zhang, Y.-L. Pi, and M. A. Bradford. Experimental and Numerical Study of Shear Connection in Composite Beams of Steel and Steel-Fibre Reinforced Concrete. *Engineering Structures*, Vol. 215, 2020, p. 110707.
46. Liu, X., M. A. Bradford, and M. S. Lee. Behavior of High-Strength Friction-Grip Bolted Shear Connectors in Sustainable Composite Beams. *Journal of Structural Engineering*, Vol. 141, No. 6, 2015, p. 04014149.
47. AASHTO. *AASHTO-LRFD Bridge Design Specifications*. American Association of State Highway and Transportation Officials, Washington, D.C. 2014.
48. American Concrete Institute. *Building Code Requirements for Structural Concrete (ACI 318-19): An ACI Standard; Commentary on Building Code Requirements for Structural Concrete (ACI 318R-19)*. ACI Committee 318, Farmington Hills, MI: American Concrete Institute, 2020.
49. ASTM-E8/E8M-16a. *Standard Test Methods for Tension Testing of Metallic Materials*. ASTM International, West Conshohocken, PA, 2016.
50. ASTM-C1437. *Standard Test Method for Flow of Hydraulic Cement Mortar*. ASTM International, West Conshohocken, PA, 2007.
51. ASTM F3125/F3125M-19. *Standard Specification for High Strength Structural Bolts and Assemblies, Steel and Alloy Steel, Heat Treated, Inch Dimensions 120 ksi and 150 ksi Minimum Tensile Strength, and Metric Dimensions 830 MPa and 1040 MPa Minimum Tensile Strength*. ASTM, West Conshohocken, PA, 2019.
52. SSPC-SP 3. *Surface Preparation Specifications No. 3, Power Tool Cleaning*. Steel Structures Painting Council, SSPC: The Society for Protective Coatings, Pittsburgh, PA, 2018.
53. ASTM C1856/C1856M-17. *Standard Practice for Fabricating and Testing Specimens of Ultra-High Performance Concrete*. ASTM International, West Conshohocken, PA, 2017.
54. ASTM-C109/C109M-21. *Standard Test Method for Compressive Strength of Hydraulic Cement Mortars (Using 2-in. or [50 mm] Cube Specimens)*. ASTM International, West Conshohocken, PA, 2021.
55. ASTM-C496-96. *Standard Test Method for Splitting Tensile Strength of Cylindrical Concrete Specimens*. ASTM International, West Conshohocken, PA, 2017.
56. AISC. *Steel Construction Manual*, 15th ed. American Institute of Steel Construction, Chicago, IL, 2017.
57. EN1994-Eurocode-4. *Design of Composite Steel and Concrete Structures*. Report of Steel Construction Institute, Berkshire, 1994.